

Realizing and Probing Baryonic Excitations in Rydberg Atom Arrays

Fangli Liu,^{1,*} Seth Whitsitt,^{1,*} Przemyslaw Bienias,¹ Rex Lundgren,¹ and Alexey V. Gorshkov¹

¹*Joint Quantum Institute and Joint Center for Quantum Information and Computer Science,
NIST/University of Maryland, College Park, MD, 20742, USA*

(Dated: January 7, 2022)

We propose a realization of mesonic and baryonic quasiparticle excitations in Rydberg atom arrays with programmable interactions. Recent experiments have shown that such systems possess a \mathbb{Z}_3 -ordered crystalline phase whose low-energy quasiparticles are defects in the crystalline order. By engineering a \mathbb{Z}_3 -translational-symmetry breaking field on top of the Rydberg-blockaded Hamiltonian, we show that different types of defects experience confinement, and as a consequence form mesonic or baryonic quasiparticle excitations. We illustrate the formation of these quasiparticles by studying a quantum chiral clock model related to the Rydberg Hamiltonian. We then propose an experimental protocol involving out-of-equilibrium dynamics to directly probe the spectrum of the confined excitations. We show that the confined quasiparticle spectrum can limit quantum information spreading in this system. This proposal is readily applicable to current Rydberg experiments, and the method can be easily generalized to more complex confined excitations (e.g. ‘tetraquarks’, ‘pentaquarks’) in phases with \mathbb{Z}_q order for $q > 3$.

The development of controllable and coherent quantum simulators has the potential to provide new insights into a variety of many-body systems [1]. Such simulators are ideal for studying phenomena such as non-equilibrium physics or scattering in quantum field theories which are difficult to simulate classically [2–6]. One class of quantum many-body systems that has been of interest recently is those exhibiting confinement. Confinement is the phenomenon whereby the fundamental excitations of a system experience a potential which increases indefinitely with their separation, resulting in the formation of bound states in the low-energy spectrum [7–9]. This mechanism plays an important role in quantum chromodynamics (QCD), where confinement due to gauge fluctuations explains the formation of mesons and baryons from quarks. Although confinement between quarks is well-established, there are a number of difficulties in obtaining quantitative estimates for physical observables [10].

Recently, there have been theoretical [11–16] and experimental [17] works on quantum simulators realizing confinement. Such quantum simulators realize experimental control over isolated quantum systems at the single-atom level, which allows a great deal of sensitivity in both manipulation and detection [18–20]. To date, these systems only exhibit pairwise confinement of particle-antiparticle pairs into mesonic two-particle bound states [21]. To make closer contact with the phenomenology of QCD, it would be advantageous to realize a model Hamiltonian whose spectrum contains more complex bound states.

In this work, we propose a quantum simulator scheme to implement confined baryonic and mesonic excitations in Rydberg atom arrays. The basis for our proposal involves the recent realization of crystalline states which exhibit spontaneously broken \mathbb{Z}_q symmetry, where the chain is populated by a Rydberg excitation every q sites [18, 22]. The low-energy excitations above these ground

states are defects which lie between the degenerate ordered ground states, and these defects may be separated from each other to arbitrary distances. We show that by adding a non-uniform on-site detuning which breaks the \mathbb{Z}_q symmetry, the different types of domain-wall defects observed in Ref. [22] are bound together so that the low-energy excitations are instead composite objects such as mesons or baryons. We demonstrate that the masses of these confined quasiparticles have a clear signature in the out-of-equilibrium dynamics of the Hamiltonian, and that the correlation spreading of the system is dramatically reduced in the confined phase. We also discuss in detail the initial state preparation and measurement scheme for observing these confined quasiparticles.

The model.— We study a one-dimensional array of Rydberg atoms described by the following Hamiltonian [18]:

$$H_{\text{Ryd}} = \sum_i \frac{\Omega_i}{2} X_i - \sum_i \Delta_i n_i + \sum_{i < j} V_{|i-j|} n_i n_j. \quad (1)$$

Here, $|r_i\rangle$ ($|g_i\rangle$) denotes the Rydberg (ground) state for atom at site i (Fig. 1), $X_i = |g_i\rangle\langle r_i| + |r_i\rangle\langle g_i|$, $n_i = |r_i\rangle\langle r_i|$, Ω_i and Δ_i are the Rabi frequencies and detunings respectively, and $V_{|i-j|}$ describes the interaction between atoms in the Rydberg state at sites i and j . The interactions decay strongly with distance, with the scaling $V_r \propto 1/r^6$. When both the Rabi frequencies and detunings are homogeneous in space, this Hamiltonian features ordered ground states where every q th site of the lattice is in the Rydberg state ($q \geq 2$) [23–26]. Recent experiments have studied the quantum many-body dynamics governed by this Hamiltonian with homogeneous parameters [18], giving insight into phenomena such as quantum many-body scars [27, 28], exotic quantum criticality [23, 25, 29], and the quantum Kibble-Zurek mechanism [22].

Relation to the \mathbb{Z}_3 chiral clock model.— We focus on

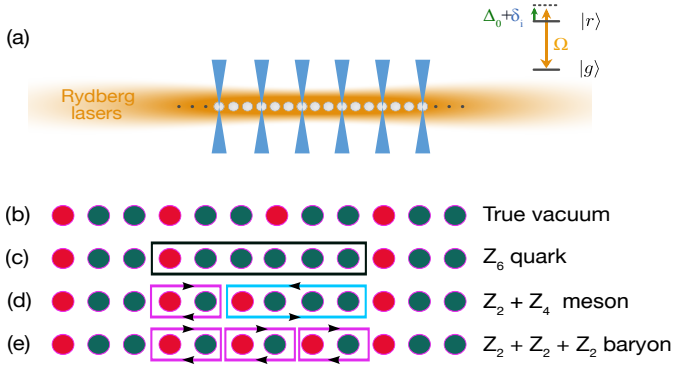


FIG. 1. (a) Implementation of symmetry breaking fields in the Rydberg array. The beams applied on every third atom create an additional detuning δ_i that is a nonzero constant only on these atoms. (b)-(e) Schematics of mesonic and baryonic excitations formed in the Rydberg array. The red and green dots denote Rydberg and ground states, respectively. With the symmetry breaking fields, different types of low-energy excitations can exist on top of (b) the true vacuum state, including (c) a \mathbb{Z}_6 quark excitation, (d) a mesonic excitation formed by $\mathbb{Z}_2 + \mathbb{Z}_4$ defects, and (e) a baryonic excitation formed by $\mathbb{Z}_2 + \mathbb{Z}_2 + \mathbb{Z}_2$ defects.

the \mathbb{Z}_3 phase of the Rydberg Hamiltonian by specializing to the case where both Ω_i and Δ_i are much smaller than V_1 . The low-energy quasiparticles above the ordered ground state [which is shown in Fig. 1(b)] are \mathbb{Z}_2 and \mathbb{Z}_4 domain walls between regions with \mathbb{Z}_3 order [see Fig. 1(d-e)] [22]. We mention that these different types of domain walls (for the homogeneous case) have been directly observed in recent experiments [22]. At higher energies, one expects to furthermore get \mathbb{Z}_q domain walls for $q > 4$ [see, for example, Fig. 1(c)].

The system which displays similar physics with the ordered Rydberg system is the three-state quantum chiral clock model [30, 31]

$$H_{\text{CCM0}} = -f \sum_j \tau_j^\dagger - J \sum_j \sigma_j^\dagger \sigma_{j+1} e^{-i\theta} + \text{h.c.}, \quad (2)$$

where θ is a phase factor, and the operators τ and σ commute on different sites, with the matrix representation

$$\sigma = \begin{pmatrix} 1 & 0 & 0 \\ 0 & \omega & 0 \\ 0 & 0 & \omega^2 \end{pmatrix}, \quad \tau = \begin{pmatrix} 0 & 0 & 1 \\ 1 & 0 & 0 \\ 0 & 1 & 0 \end{pmatrix}, \quad (3)$$

where $\omega = e^{2\pi i/3}$. The clock model obeys a \mathbb{Z}_3 symmetry generated by the operator $\mathcal{G} = \prod_i \tau_i$, and the ground states ('vacua') are three-fold degenerate in the ordered phase. Consequently, the elementary excitations are the clockwise or anti-clockwise domain walls between any two different types of the three vacua [see Fig. 2]. Because of the degeneracy, the domain walls may be separated to infinity, since moving a domain wall costs no energy. For $\theta = 0$, the two lowest defects have the same excitation

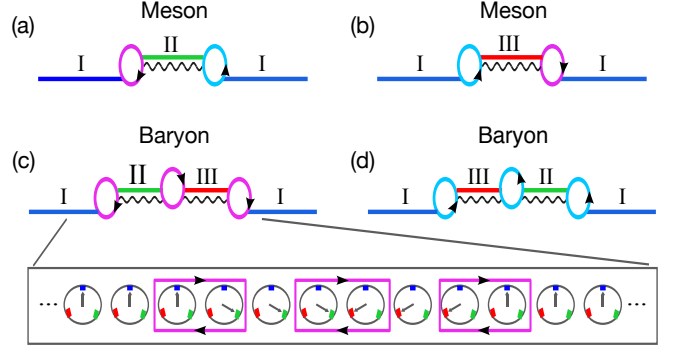


FIG. 2. Schematics of mesonic and baryonic excitations formed by the three different vacua in the confined chiral clock model, Eq. (4). The different vacua are labelled by straight lines with different colors, and the clockwise (anti-clockwise) domain walls between two vacua are labelled by magenta (cyan) circles. The energy cost for creating domain walls scales linearly with their distances, as illustrated by the wavy line. For (c), we additionally give a schematic of the baryonic excitation in the clock basis.

energy, and Eq. (2) is the ordinary three-state quantum Potts model, while when $\theta \neq 0$, the two domain walls will have differing energies. Because the lowest-energy excitations have the same structure, the phase transitions in the clock and Rydberg models lie in the same universality class [24, 25, 29]. Such clock models have been used to study low-energy confinement in a number of previous works [8, 32–36], so we shall use intuition obtained from these works to understand how confinement can be engineered in the Rydberg arrays.

Confinement via spatially periodic detunings.— We now consider an additional spatially periodic detuning δ_i on top of the homogeneous Δ_0 in the Rydberg Hamiltonian. Specifically, we analyze the case where there is an energy decrease of the Rydberg state for every third atom [see Fig. 1(a)]. The periodic field can be realized in experiments by using locally addressed lasers [37]. With this field, the three-fold degeneracy of the vacua and the \mathbb{Z}_3 symmetry of Eq. (2) [and Eq. (1)] are explicitly broken [see Fig. 2]. We use I to label the ‘true vacuum’ which has lower energy than the other two degenerate ‘false vacua’ II and III. The corresponding quantum clock Hamiltonian now includes an additional longitudinal field

$$H_{\text{CCM1}} = -f \sum_j \tau_j^\dagger - J \sum_j \sigma_j^\dagger \sigma_{j+1} e^{-i\theta} - h \sum_j \sigma_j + \text{h.c.} \quad (4)$$

In contrast to the homogeneous case, with the longitudinal field, the domain-walls between true and false vacua cannot be separated to long distances due to a confining potential (an energy penalty) which scales linearly with the separation between defects. Consequently, the low-energy excitations of the Hamiltonian for large system sizes must be entirely made up of bound states of

domain walls. This is in close analogy to confinement in particle physics, where quarks cannot be directly observed in nature as two (three) of them are bound into mesons (baryons), due to similar confining potential scaling [7–9].

Fig. 2 schematically shows the low-energy bound quasiparticle excitations formed by different vacua, which include both mesonic and baryonic bound states. The mesonic states are formed by two domain walls, including one clockwise (connecting $I \rightarrow II$, $II \rightarrow III$, or $III \rightarrow I$) and one counterclockwise (connecting $III \rightarrow II$, $II \rightarrow I$, or $I \rightarrow III$) defect [Fig. 2(a-b)]. On the other hand, the baryonic excitations are composed of either three clockwise domain walls or three anti-clockwise domain walls [see Fig. 2(c-d)].

A schematic plot of the low energy excitations on top of the true ground state for the Rydberg array is shown in Fig. 1, where the picture is exact when $\Omega = 0$. The ordered ground state is mapped to the \mathbb{Z}_3 -ordered crystalline state for the Rydberg chain [Fig. 1(b)]. Further, the clockwise and anti-clockwise defects map to the \mathbb{Z}_2 and \mathbb{Z}_4 defects, respectively [Fig. 1(d)]. Due to the same mechanism, the additional real-space periodic potential leads to a confining potential between the domain walls, which thus leads to bound states of the \mathbb{Z}_2 and \mathbb{Z}_4 defects. It is clear that both the mesonic and baryonic excitations shown in Fig. 2 can be mapped to corresponding Rydberg configurations. We note that the Rydberg model of Eq. (1) will additionally allow higher-energy defect states such as “ \mathbb{Z}_6 quarks” [Fig. 1(c)], which have no analogue in the chiral clock model.

Although we have focused on the \mathbb{Z}_3 case, the above can be formulated for any of the \mathbb{Z}_q ordered states. For $q = 2$, this corresponds to the well-studied confinement in the Ising model with a longitudinal field [9, 16]. For $q > 3$, one can additionally obtain more complicated ‘tetraquark’ or ‘pentaquark’ states, in which 4 or 5 domain walls, respectively, bind together. We note that the spectrum of confined excitations for the Potts [$\theta = 0$ in Eq. (4)] model has been explored in a number of theoretical works [33–36], but the general $\theta \neq 0$ case has not been explored yet. While our proposal to realize confinement does not come from a lattice gauge theory, the relation between confinement in spin models and gauge theories has a long history in the nonperturbative study of lattice gauge theories [7, 8, 38, 39]. This is particularly clear in one dimension, where the mechanism of confinement in gauge theories can be similarly described as binding together defects between degenerate vacua, although resulting from matter coupling to gauge field [40, 41]. In fact, the \mathbb{Z}_2 case for our present system is dual to the bosonized massive Schwinger model [42, 43].

Detecting quasiparticle masses.—We consider using quench dynamics to probe ‘mesonic’ and ‘baryonic’ masses in Rydberg experiments. One can in principle prepare the product state of Fig. 1(b), and the subse-

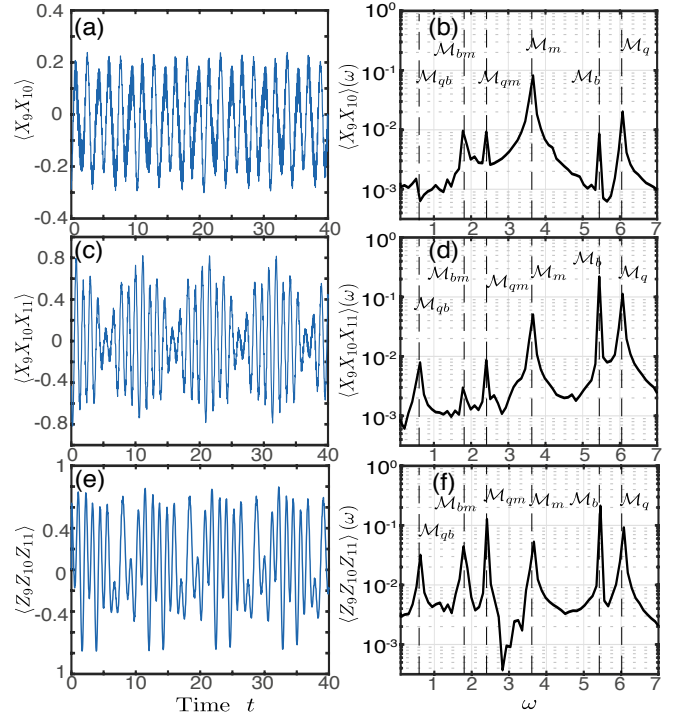


FIG. 3. (a-b) The initial state is chosen to maximize the total probability of $|\Psi_v\rangle$ and $|\Psi_m\rangle$ under the preparation protocol discussed in the text. (c-f) The initial state is chosen to maximize total probability $|\Psi_v\rangle$ and $|\Psi_b\rangle$. Shown are the time-dependent expectation values and the associated Fourier spectra of (a-b) $\langle \Psi(t) | X_9 X_{10} | \Psi(t) \rangle$, (c-d) $\langle \Psi(t) | X_9 X_{10} X_{11} | \Psi(t) \rangle$, and (e-f) $\langle \Psi(t) | U^\dagger Z_9 Z_{10} Z_{11} U | \Psi(t) \rangle$, where U is a $\pi/2$ -pulse applied to the middle three atoms. The dotted lines denote the energy of the meson (\mathcal{M}_m), baryon (\mathcal{M}_b), quark (\mathcal{M}_q) and their energy differences (\mathcal{M}_{bm} , \mathcal{M}_{qm} , \mathcal{M}_{qb}) obtained from exact diagonalization. Parameters: $L = 18$, Ω_i is chosen to be homogeneous $\Omega = 1$; $\Delta_i = \Delta_0 + \delta_i$, where $\Delta_0 = 4$ and $\delta_i = 2$ for $(i \bmod 3) = 1$ and 0 otherwise; $V_1 = 164.17$, corresponding to Rydberg radius being 2.34 [22].

quent quench dynamics under Eq. (1) would be set by the excitation energies of the bound quasiparticles [9]. However, since we work in the regime where Ω is much smaller than Δ and V_2 , the excitation probability of bound quasiparticles can be low as it intrinsically involves high-order processes [44].

We instead choose the initial states to have sizable overlap with both the ground state and localized excited states. Since the lowest-order mesonic and baryonic excitations involve flipping the states of only three atoms (in the $\Omega_i = 0$ limit), we consider the set of initial states involving a large superposition of the true vacuum state $|\Psi_v\rangle = |\dots rggrgrgrgrgg\dots\rangle$ and the target mesonic $|\Psi_m\rangle = |\dots rggrgrgrgggrg\dots\rangle$, or involving the true vacuum state and baryonic state $|\Psi_b\rangle = |\dots rggrgrgrgrgg\dots\rangle$ (see Fig. 1)[45]. The intuition for choosing such initial states comes from the $\Omega_i = 0$ limit, where the dy-

namics with such initial states involves oscillations between the ‘true vacuum’ state and the localized mesonic and/or baryonic states displayed in Fig. 1. We will show that the real-time dynamics involving these states can indeed resolve the many-body bound excitations for general $\Omega_i \neq 0$ [Fig. 3].

We first choose the time-dependent observables to be $X_9X_{10}X_{11}$ and X_9X_{10} (chain length $L = 18$), as they have non-vanishing matrix elements between the vacuum state and the baryonic and mesonic state, respectively. Fig. 3 shows the numerical results for the time-dependent expectation value of observables and their Fourier transform. Note that the initial state is chosen to maximize the total probability of $|\Psi_v\rangle$ and $|\Psi_m\rangle$ [for Fig. 3(a-b)], or the total probability of $|\Psi_v\rangle$ and $|\Psi_b\rangle$ [for Fig. 3(c-d)], under a specific preparation protocol (discussed later). These states are evolved under the fully long-range Hamiltonian Eq. (1) with non-zero δ_i , and other parameters are chosen such that the ground state is in the \mathbb{Z}_3 -ordered phase for $\delta_i = 0$. As Figs. 3(a) and (c) show, the observables exhibit clear periodic oscillations. Their Fourier spectra [Fig. 3(b) and (d)] agree perfectly with the masses of the ‘ $\mathbb{Z}_2 + \mathbb{Z}_4$ meson’ (\mathcal{M}_m), the ‘ $\mathbb{Z}_2 + \mathbb{Z}_2 + \mathbb{Z}_2$ baryon’ (\mathcal{M}_b), the ‘ \mathbb{Z}_6 quark’ (\mathcal{M}_q), and their energy differences (\mathcal{M}_{bm} , \mathcal{M}_{qb} and \mathcal{M}_{qm}). We mention that the highest Fourier peaks of Fig. 3(b) and (d) agree with the mesonic and baryonic masses respectively, as the particular initial states have large components of the target excited states.

We note that in the current experiments only measurement in the Z -basis is possible. In order to access the masses given by X -observables, one can use a $\pi/2$ pulse (which we denote as U) rotating the states of the middle three atoms before the measurement (subject to Rydberg constraint as discussed in detail later). The observable $\langle \Psi(t) | U^\dagger Z_9 Z_{10} Z_{11} U | \Psi(t) \rangle$ after the rotation also oscillates with a large contrast [see Figs. 3(e)], and its Fourier spectrum accurately determines the masses of the baryonic, mesonic and the higher-energy quark excitations [Figs. 3(f)]

Quantum information spreading.—The confined quasiparticles at low energy can have a dramatic effect on the correlation spreading in the system. For instance, confinement can strongly suppress the spreading of correlations and lead to slow thermalization [9, 46]. Here we focus on the time-dependent connected correlation function $|\langle n_j n_k \rangle_c| = |\langle n_j n_k \rangle - \langle n_j \rangle \langle n_k \rangle|$ to study the quantum information spreading after a quantum quench from an initial \mathbb{Z}_3 -ordered product state. Fig. 4(a) shows the case of a homogeneous post-quench Hamiltonian with $\delta_i = 0$. As one can clearly see, correlations spread out fast across the 1D chain, leading to a light-cone structure [47]. In contrast, with a periodic detuning field added to the Hamiltonian, the low-energy excitations are bound quasiparticles (mesons and baryons). In this case, the correlation spreads much slower than in the deconfined

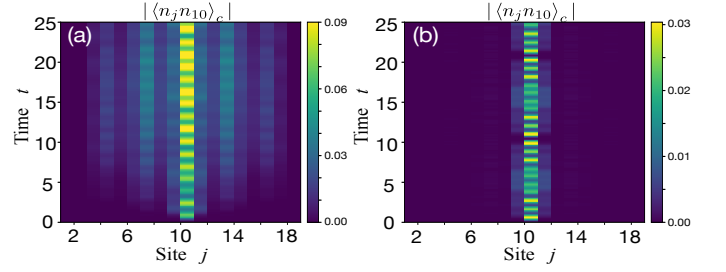


FIG. 4. Correlation spreading after a quantum quench from the \mathbb{Z}_3 -ordered state $|\Psi_v\rangle$. (a) shows the time-dependent $|\langle n_j n_{10} \rangle_c|$ without the additional periodic spatially detuning, i.e. $\delta_i = 0$. (b) shows the same quantity with $\delta_i = 2$ for $(i \bmod 3) = 1$ and 0 otherwise. All other parameters are the same for (a) and (b): $\Omega = 1, \Delta_0 = 4, V_1 = 164.17, L = 19$.

case [see Fig. 4(b)]. We emphasize that such observables can also be directly measured in experiments [18, 22].

Experimental preparation and detection.—To experimentally prepare the above sets of initial states, one can first prepare the ordered product state $|\Psi_v\rangle = |rggrggrggrggrggrg\rangle$ [18, 22], and rotate the 10th atom from the Rydberg to the ground state (via single-atom addressability), which yields $|\Psi_q\rangle = |rggrggrgggggrggrg\rangle$ [48]. After this, a Rabi laser is shined only on the middle three atoms, with a Rabi frequency Ω_0 satisfying $V_2 \ll \Omega_0 \ll V_1$. To prepare the initial state for Fig. 3(a-b), we apply the Rabi pulse for time $1.4\pi/\Omega_0$. On the other hand, for the initial states in Fig. 3(c-f), we choose time $3.6\pi/\Omega_0$. During the preparation, the parameters Δ and interactions V_r are the same as in the post-quenched Hamiltonian [see Fig. 3], while $\Omega_0 = 25$ for the three atoms, and all other atoms seeing vanishing Rabi frequencies. We have checked that the probabilities for the blockaded states (grr, rrg, rrr) for the three middle atoms are on the order of 10^{-3} .

To measure the dynamics shown in Fig. 3(e-f), after state preparation, we evolve the system under Hamiltonian (1), rotate the middle three atoms back using a $\pi/2$ pulse [i.e. apply Ω_0 for time $\pi/(2\Omega_0)$], and finally measure $Z_9 Z_{10} Z_{11}$. During the $\pi/2$ pulse, all the parameters (except for the pulse time) are the same as for the preparation step.

Conclusions and outlook.—Our proposal shows that Rydberg arrays are a natural platform to study exotic confined excitations not only for the mesonic case, but also for baryonic quasiparticles. These confined excitations are analogous to the more complicated bound states seen in high energy physics. Although we focus on the regime where the Rydberg system is described by an effective clock model, we expect Eq. (1) to exhibit confinement wherever the homogeneous Rydberg model is in the \mathbb{Z}_3 ordered phase. Away from the clock limit, one needs to consider more general \mathbb{Z}_q defect states where $q > 4$, and this will lead to more complicated ‘hadronic’

excitations. Correspondingly, this analysis can be generalised to the other \mathbb{Z}_q -ordered phases of the Rydberg system, which will generally lead to a host of more complicated confined quasiparticles (e.g. ‘tetraquarks’ and ‘pentaquarks’). These more complex states would require much larger system sizes which would no longer be amenable to the numerical methods used here, but can be achieved in quantum simulators. Quantum simulators can additionally access dynamical phenomena such as string breaking and inelastic scattering which are intractable using classical methods [4]. It would also be interesting to consider confinement scenarios in higher dimensions, where Rydberg systems feature more complicated phases of crystalline order [49]. In particular, the symmetry-breaking patterns in two dimensions allow for both one-dimensional domain wall excitations as well as point-like “monopole” excitations, which is similar to the distinct excitations in higher-dimensional gauge theories [39].

We thank Zohreh Davoudi, Sepehr Ebadi, Markus Heyl, Alexander Keesling, Mikhail Lukin, Ahmed Omran, and Roberto Verdel for insightful discussions. PB thanks ITAMP for hospitality and support via the Visitor Program. This work was supported by AFOSR, AFOSR MURI, DoE BES Materials and Chemical Sciences Research for Quantum Information Science program (award No. DE-SC0019449), DoE ASCR Quantum Testbed Pathfinder program (award No. DE-SC0019040), DoE ASCR Accelerated Research in Quantum Computing program (award No. DE-SC0020312), NSF PFCQC program, ARO MURI, ARL CDQI, and NSF PFC at JQI.

* These authors contributed equally to this work. Correspondence to: fliu1235@umd.edu (F.L.); spwhitsitt@gmail.com (S.W.)

- [1] J. I. Cirac and P. Zoller, “Goals and opportunities in quantum simulation,” *Nat. Phys.* **8**, 264 (2012).
- [2] J. Eisert, M. Friesdorf, and C. Gogolin, “Quantum many-body systems out of equilibrium,” *Nat. Phys.* **11**, 124 (2015).
- [3] C. Gogolin and J. Eisert, “Equilibration, thermalisation, and the emergence of statistical mechanics in closed quantum systems,” *Rep. Prog. Phys.* **79**, 056001 (2016).
- [4] J. Preskill, “Simulating quantum field theory with a quantum computer,” in *The 36th Annual International Symposium on Lattice Field Theory. 22-28 July* (2018) [arXiv:1811.10085 \[hep-lat\]](#).
- [5] S. P. Jordan, K. S. M. Lee, and J. Preskill, “Quantum Computation of Scattering in Scalar Quantum Field Theories,” *Quantum Inf. Comput.* **2**, 1014 (2014).
- [6] S. P. Jordan, H. Krovi, K. S. M. Lee, and J. Preskill, “BQP-completeness of scattering in scalar quantum field theory,” *Quantum* **2**, 44 (2018).
- [7] J. B. Kogut, “An introduction to lattice gauge theory and spin systems,” *Rev. Mod. Phys.* **51**, 659 (1979).
- [8] B. M. McCoy and T. T. Wu, “Speculations on quark observation,” *Phys. Lett. B* **72**, 219 (1977).
- [9] M. Kormos, M. Collura, G. Takács, and P. Calabrese, “Real-time confinement following a quantum quench to a non-integrable model,” *Nat. Phys.* **13**, 246 (2017).
- [10] N. Brambilla *et al.*, “QCD and Strongly Coupled Gauge Theories: Challenges and Perspectives,” *Eur. Phys. J. C* **74**, 2981 (2014).
- [11] F. M. Surace, A. Russomanno, M. Dalmonte, A. Silva, R. Fazio, and F. Iemini, “Floquet time crystals in clock models,” *Phys. Rev. B* **99**, 104303 (2019).
- [12] M. C. Bañuls, R. Blatt, J. Catani, A. Celi, J. I. Cirac, M. Dalmonte, L. Fallani, K. Jansen, M. Lewenstein, S. Montangero, C. A. Muschik, B. Reznik, E. Rico, L. Tagliacozzo, K. Van Acoleyen, F. Verstraete, U. J. Wiese, M. Wingate, J. Zakrzewski, and P. Zoller, “Simulating Lattice Gauge Theories within Quantum Technologies,” [arXiv:1911.00003](#).
- [13] H. Weimer, M. Müller, I. Lesanovsky, P. Zoller, and H. P. Büchler, “A Rydberg quantum simulator,” *Nat. Phys.* **6**, 382 (2010).
- [14] S. Notarnicola, M. Collura, and S. Montangero, “Real-time-dynamics quantum simulation of (1+1)-dimensional lattice qed with rydberg atoms,” *Phys. Rev. Research* **2**, 013288 (2020).
- [15] G. Magnifico, M. Dalmonte, P. Facchi, S. Pascazio, F. V. Pepe, and E. Ercolessi, “Real Time Dynamics and Confinement in the \mathbb{Z}_n Schwinger-Weyl lattice model for 1+1 QED,” [arXiv:1909.04821](#).
- [16] F. Liu, R. Lundgren, P. Titum, G. Pagano, J. Zhang, C. Monroe, and A. V. Gorshkov, “Confined quasiparticle dynamics in long-range interacting quantum spin chains,” *Phys. Rev. Lett.* **122**, 150601 (2019).
- [17] W. L. Tan, P. Becker, F. Liu, G. Pagano, K. S. Collins, A. De, L. Feng, H. B. Kaplan, A. Kyprianiadis, R. Lundgren, W. Morong, S. Whitsitt, A. V. Gorshkov, and C. Monroe, “Observation of Domain Wall Confinement and Dynamics in a Quantum Simulator,” [arXiv:1912.11117](#).
- [18] H. Bernien, S. Schwartz, A. Keesling, H. Levine, A. Omran, H. Pichler, S. Choi, A. S. Zibrov, M. Endres, M. Greiner, V. Vuletić, and M. D. Lukin, “Probing many-body dynamics on a 51-atom quantum simulator,” *Nature* **551**, 579 (2017).
- [19] D. Barredo, V. Lienhard, S. de Léséleuc, T. Lahaye, and A. Browaeys, “Synthetic three-dimensional atomic structures assembled atom by atom,” *Nature* **561**, 79 (2018).
- [20] I. Bloch, J. Dalibard, and S. Nascimbène, “Quantum simulations with ultracold quantum gases,” *Nat. Phys.* **8**, 267 (2012).
- [21] Baryonic bound states have been proposed in Ref. 50, but this model does not exhibit confinement.
- [22] A. Keesling, A. Omran, H. Levine, H. Bernien, H. Pichler, S. Choi, R. Samajdar, S. Schwartz, P. Silvi, S. Sachdev, P. Zoller, M. Endres, M. Greiner, Vuletić, V. , and M. D. Lukin, “Quantum Kibble-Zurek mechanism and critical dynamics on a programmable Rydberg simulator,” *Nature* **568**, 207 (2019).
- [23] M. Rader and A. M. Läuchli, “Floating Phases in One-Dimensional Rydberg Ising Chains,” [arXiv:1908.02068](#).
- [24] P. Fendley, K. Sengupta, and S. Sachdev, “Competing density-wave orders in a one-dimensional hard-boson model,” *Phys. Rev. B* **69**, 075106 (2004).
- [25] R. Samajdar, S. Choi, H. Pichler, M. D. Lukin, and

- S. Sachdev, “Numerical study of the chiral \mathbb{Z}_3 quantum phase transition in one spatial dimension,” *Phys. Rev. A* **98**, 023614 (2018).
- [26] N. Chepiga and F. Mila, “Floating phase versus chiral transition in a 1d hard-boson model,” *Phys. Rev. Lett.* **122**, 017205 (2019).
- [27] C. J. Turner, A. A. Michailidis, D. A. Abanin, M. Serbyn, Papić, and Z. , “Weak ergodicity breaking from quantum many-body scars,” *Nat. Phys.* **14**, 745 (2018).
- [28] W. W. Ho, S. Choi, H. Pichler, and M. D. Lukin, “Periodic orbits, entanglement, and quantum many-body scars in constrained models: Matrix product state approach,” *Phys. Rev. Lett.* **122**, 040603 (2019).
- [29] S. Whitsitt, R. Samajdar, and S. Sachdev, “Quantum field theory for the chiral clock transition in one spatial dimension,” *Phys. Rev. B* **98**, 205118 (2018).
- [30] S. Ostlund, “Incommensurate and commensurate phases in asymmetric clock models,” *Phys. Rev. B* **24**, 398 (1981).
- [31] D. A. Huse and M. E. Fisher, “Domain walls and the melting of commensurate surface phases,” *Phys. Rev. Lett.* **49**, 793 (1982).
- [32] A. B. Zamolodchikov, “Integrals of motion and s-matrix of the (scaled) $t = t_c$ ising model with magnetic field,” *Int. J. Mod. Phys. A* **04**, 4235 (1989).
- [33] G. Delfino and P. Grinza, “Confinement in the q-state potts field theory,” *Nucl. Phys. B* **791**, 265 (2008).
- [34] L. Lepori, G. Z. Tóth, and G. Delfino, “The particle spectrum of the three-state Potts field theory: a numerical study,” *J. Stat. Mech.: Theory Exp* **2009**, 11007 (2009).
- [35] S. B. Rutkevich, “Baryon masses in the three-state Potts field theory in a weak magnetic field,” *J. Stat. Mech.: Theory Exp* **2015**, 01010 (2015).
- [36] M. Lencsés and G. Takács, “Confinement in the q-state Potts model: an RG-TCSA study,” *J. High Energy Phys* **2015**, 146 (2015).
- [37] A. Omran, H. Levine, A. Keesling, G. Semeghini, T. T. Wang, S. Ebadi, H. Bernien, A. S. Zibrov, H. Pichler, S. Choi, J. Cui, M. Rossignolo, P. Rembold, S. Montangero, T. Calarco, M. Endres, M. Greiner, V. Vuletić, and M. D. Lukin, “Generation and manipulation of schrödinger cat states in rydberg atom arrays,” *Science* **365**, 570 (2019).
- [38] S. Elitzur, R. B. Pearson, and J. Shigemitsu, “Phase structure of discrete abelian spin and gauge systems,” *Phys. Rev. D* **19**, 3698 (1979).
- [39] M. B. Einhorn, R. Savit, and E. Rabinovici, “A physical picture for the phase transitions in zn symmetric models,” *Nucl. Phys. B* **170**, 16 (1980).
- [40] S. Coleman, R. Jackiw, and L. Susskind, “Charge shielding and quark confinement in the massive schwinger model,” *Ann. Phys.* **93**, 267 (1975).
- [41] S. Coleman, “More about the massive schwinger model,” *Ann. Phys.* **101**, 239 (1976).
- [42] G. Delfino and G. Mussardo, “Non-integrable aspects of the multi-frequency sine-gordon model,” *Nucl. Phys. B* **516**, 675 (1998).
- [43] R. Shankar and G. Murthy, “Deconfinement in $d = 1$: Asymptotic and half-asymptotic particles,” *Phys. Rev. B* **72**, 224414 (2005).
- [44] The transition from the vacuum state to the mesonic (baryonic) excitation involves a second (third) order process.
- [45] The ‘...’ denotes repeated structure of the ordered phase with rgg.
- [46] Z.-C. Yang, F. Liu, A. V. Gorshkov, and T. Iadecola, “Hilbert-space fragmentation from strict confinement,” *Phys. Rev. Lett.* **124**, 207602 (2020).
- [47] The light-cone shows a \mathbb{Z}_3 -periodic sub-structure due to the blockade physics.
- [48] The local rotation fields can be also engineered by applying a strong light shift to the selected target atoms, and shining an additional resonant Rydberg laser beam across the whole chain.
- [49] R. Samajdar, W. W. Ho, H. Pichler, M. D. Lukin, and S. Sachdev, “Complex density wave orders and quantum phase transitions in a model of square-lattice rydberg atom arrays,” *Phys. Rev. Lett.* **124**, 103601 (2020).
- [50] Á. Rapp, G. Zaránd, C. Honerkamp, and W. Hofstetter, “Color superfluidity and ”baryon” formation in ultracold fermions,” *Phys. Rev. Lett.* **98**, 1 (2007).